Hemodynamic Studies of Intracranial Dural Arteriovenous Fistulas Using Arterial Spin-labeling MR Imaging

T. NOGUCHI[1], H. IRIE[1], Y. TAKASE[2], M. KAWASHIMA[2], T. OOTSUKA[1], M. NISHIHARA[1], Y. EGASHIRA[1], J. NOJIRI[1], T. MATSUSHIMA[2], S. KUDO[1]

[1] Department of Radiology, [2] Neurosurgery, Faculty of Medicine, Saga University; Nabeshima, Saga, Japan

Keywords: MRI, arterial spin-labeling, PASL, intracranial dural arteriovenous fistula, perfusion, SPECT

Summary

Arterial spin-labeling (ASL) magnetic resonance imaging (MRI) enables non-invasive acquisition of the brain perfusion information in cerebrovascular disease. We investigated hemodynamic changes in intracranial dural arteriovenous fistulas (DAVFs) using ASL-MRI.

ASL-MRI by a Q2TIPS sequence on a 3.0-Tesla MRI was performed for three patients with Cognard's IIa+b type of DAVFs before and after treatment. Perfusion images obtained by ASL-MRI (ASL images) before treatment were visually compared with those by single-photon emission computed tomography images (SPECT images). Increasing rates of temporal changes of regional perfusion values in ASL images (ASL values) before and after treatment were also calculated.

In all three patients, ASL images before treatment demonstrated high perfusion in regions around the shunting areas, where normal or low perfusion were detected on SPECT images; thus, ASL images might have demonstrated the abundant arterial shunting flow via the fistulas. On days eight to 20 after treatment, ASL values around the shunt areas remained the same or decreased, and those in the regions other than the shunt areas increased in all three patients. This might have been due to a combination of the following: a decrease in shunt flow volume, an amelioration of venous congestion, and a sustained an upward shift in the autoregulation of the brain perfusion pressure. All regional ASL values decreased on days 112 and 120 after treatment in two patients, which possibly reflects a reduction in the upward shift in autoregulation.

ASL-MRI might be useful for identifying the hemodynamic behavior of DAVFs before and after treatment.

Introduction

The pathology of intracranial dural arteriovenous fistulas (DAVFs) is the presence of arteriovenous shunts within the dura [1-3]. It has been reported that the venous hypertension and obstruction of the venous drainage induced by the abnormal arterial blood flow supplied via shunts occasionally provoke central nervous disorders such as venous infarction, intracranial hemorrhage, and other neurological deficits [4-10]. Several authors have described the cerebral perfusion abnormalities in patients with DAVFs which were improved after treatment [4-6]. Single-photon emission computed tomography (SPECT) and positron emission tomography (PET) have been applied to examine the hemodynamic features of DAVFs [11-14]. However, the frequent evaluations are hindered by factors such as expense, cumbersome procedures, and drug-induced side-effects.

Arterial spin-labeling (ASL) magnetic resonance imaging (MRI) is one of brain perfusion imaging methods on MRI and able to generate brain perfusion images without the injection of the extrinsic tracer [15-19]. ASL-MRI will facilitate the frequent and noninvasive acquisitions of the perfusion information, which is expected

to be helpful for evaluating the temporal hemodynamic changes in DAVFs. Moreover, ASL-MRI is sensitive to the blood flow in larger arteries as well as that in capillaries. We performed ASL-MRI to patients with DAVFs and found that it could demonstrate temporal changes in not only brain perfusion but also arterial shunting flows. In this study, we estimated the clinical applicability of ASL-MRI in patients with DAVFs.

Materials and Methods

The current retrospective research was approved by our institutional review board (Receipt No.21-43, 2009).

Patients

From May to August 2008, three patients with DAVFs were admitted to our hospital. Table 1 showed the profiles of these three patients.

Patient 1 was a 60-year-old woman manifesting aphasia and conversational impairment. Digital subtraction angiography (DSA) revealed the arterial blood flowing from the bilateral occipital arteries, left posterior auricular artery, left middle meningeal artery, and left accessory meningeal artery directly into the torcular Herophili - left transverse - sigmoid sinus, and then draining into the left superior petrosal - cavernous sinus - cortical vein and the left-sided Labbe's vein in a retrograde fashion, and the right transverse-sigmoid sinus in an antegrade fashion (Cognard's IIa+b type / Lalwani's grade 3). Head MRI revealed a suspected venous infarction at the left temporal lobe where the abnormal findings were shown including the dilated vessels along the cerebral surface and the increased signal on T2-weighted images. Transcatheter arterial embolization by N-butyl-2-cyanoacrylate (NBCA) through all of the feeding arteries was performed. DSA on the tenth day after treatment showed a disappearance of the retrograde flow into cortical veins. The patient's Wechsler Adult Intelligence Scale-III (WAIS-III) score improved after treatment.

Patient 2 was a 73-year-old woman who had experienced bilateral conjunctival hyperemia. DSA showed the arterial shunting flows from the bilateral sides of the ascending pharyngeal arteries, middle meningeal arteries, and meningohypophyseal arteries into the bilateral cavernous sinuses, and then draining into the bilateral superior ophthalmic veins, left inferior ophthalmic veins, the basilar plexus in an antegrade fashion, and left uncal vein in a retrograde fashion (Cognard's IIa+b type / Barrow's D type). In particular, the retrograde flow through left uncal vein flowed into the left lentiform nucleus. Head MRI showed high intensity on the T2-weighted images, with low intensity on T2-star-weighted images of the left lentiform nucleus, which was suggestive of venous congestion. The bilateral conjunctival hyperemia disappeared within two weeks after transcatheter cavernous sinus coil embolization. Serial MRI study after treatment revealed a diminished high intensity on the T2-weighted images, and a resolution of the low intensity on the T2-star-weighted images of the left lentiform nucleus.

Patient 3 was a 64-year-old man urgently hospitalized for a general tonic convulsion. DSA enabled visualization of the arterial shunting flow from the bilateral occipital arteries, right posterior auricular artery, right middle meningeal artery, and left ascending pharyngeal artery, into the right transverse - sigmoid sinus, and then draining into the right side of the superior and inferior cerebellar hemispheric veins and the cortical veins along the temporo-parieto-occipital lobe in a retrograde fashion, and the superior sagittal and straight - left transverse - sigmoid sinuses in an antegrade fashion (Cognard's IIa+b type / Lalwani's grade 3). On MRI study, T2-prolongation with multiple flow voids was observed in both the right cerebellar hemisphere and the right temporo-parieto-occipital lobe. A small hemorrhage was identified at the right temporal lobe on CT images. The patient was initially treated with percutaneous transcatether arterial embolization. However, the retrograde cortical venous flow was still recognized. Then, the additional transcatheter right transverse - sigmoid sinus coil embolization under right suboccipital craniotomy was performed on the next day. DSA on 16th day after the initial treatment demonstrated a disappearance of the retrograde cortical venous flow. No recurrent convulsions were noted after treatment.

ASL-MRI

All ASL-MRI were performed on a clinical 3.0-Tesla MRI unit (MAGNETOM Trio, A Tim System, Siemens AG, Erlangen, Germany) with a 12-channel head coil. The perfusion images

were obtained by the second version of the quantitative imaging of perfusion using a single subtraction (QUIPSS II) MRI pulse sequence with thin-slice TI1 periodic saturation (Q2TIPS). This is a pulsed arterial spin-labeling method that enables the acquisition of multiple sections [19]. Since Q2TIPS installed on our MRI unit was one of the finished MRI sequence products and was generously provided for the clinical application, ASL-MRI was performed as a component of routine clinical brain MRI examination. ASL-MRI was performed 12-39 days before treatment (three patients), 8-20 days after treatment (three patients), and 112-120 days after treatment (two patients).

The Q2TIPS system consisted of both labeling and image-acquisition sequences. The labeling sequence had several important parameters: a labeling slab position; an imaging slab position; and three timing parameters termed TI1, TI1S and TI2 [19]. The labeling slab was the region in which proximal arterial blood was labeled by an inversion recovery (IR) radiofrequency pulse. The imaging slab was the region in which perfusion imaging data acquisition was performed. Firstly, IR pulse was performed for labeling the arterial blood on the labeling slab (the elapsed time; t = 0). The labeled arterial blood would stream toward the imaging slab with a given cerebral blood flow rate termed f. Secondly, the periodic saturation pulse was performed at the labeling slab during a given time period from TI1 to TI1S (t = TI1-TI1S). That meant that only {f × TI1} of the labeled blood volume would pass from the labeling slab to the distal part and the remaining labeled blood would be eliminated thereafter. Finally, the imaging data acquisition was performed in the imaging slab after a given time termed TI2 (t = TI2) [19-21]. The parameters of the labeling sequence are as follows: TI1 / TI1S / TI2 (ms) = 700/1800/2000; the labeling slab width / the imaging slab width / the gap between the labeling and imaging slabs (mm) = 100/114/25.

The image acquisition in the Q2TIPS system employed an echo-planar imaging (EPI) sequence. The imaging sequence had an important parameter, a flow limit. The flow limit meant the cut-off value of flow velocity of eliminating fast-moving spins by crusher gradients. If the flow limit was set to infinity, or no crusher gradients, the perfusion values would be overestimated. On the other hand, if the flow limit was set to 0 cm/s, the gain in flow accuracy would be canceled out by extended echo time (TE) and decreased signal-to-noise ratio (SNR). In our series, a flow limit = 4 cm/s was chosen as a trade-off because it was empirically confirmed that the flow distribution were more physiologically reasonable values if the flow limit were set between 1 and 5 cm/s [22]. In other words, the labeled arterial blood would be detected on ASL-MRI in any places including arteries, veins or parenchyma as long as it was less than 4 cm/s of flow velocity. The other parameters of the imaging sequence are as follows: repetition time / echo time (ms) = 2500/17; field of view (mm) = 256×256×114; slice thickness /interslice gap (mm) = 6/1.2; total slice number = 16; coverage area = whole brain; slice acquisition order = sequential, proximal-to-distal direction; matrix = 64×64; voxel size (mm) = 4×4×6; phase partial Fourier acquisition rate = 7/8; total image number = 91 (first image volume acquired without a labeling pulse as an M0 image volume, and 45 pairs of labeled and unlabeled image volumes). The acquisition time of Q2TIPS (minutes: seconds) amounted to 3: 57.

Voxel-wise calculation and subsequent mapping of the ASL images (ASL map) were performed according to the following equation for quantitative CBF, as proposed by Wang et al. [23]:

$$f = \lambda \times \delta M / (2\alpha \times M0 \times TI1 \times \exp(-TI2/T1a)),$$

Where λ is the brain/blood partition coefficient of water, δM is the difference of the longitudinal magnetization between the unlabeled and labeled images in the region of interest (ROI), α is the inversion efficiency, and T1a is the longitudinal relaxation time of blood. Here, λ, α, and T1a were assumed to be 0.9, 0.95 and 1496.19 (ms), respectively.

The intracranial regional perfusion values (ASL values) were calculated as follows: an ASL map was converted to the analyze format using the free computer software MRIcro (version 1.40 build 1, Professor Chris Rorden, Georgia Institute of Technology, Atlanta GA, USA, http://www.cabiatl.com/mricro/mricro/index.html). A normalized ASL map was created from the converted ASL map using the free computer software package SPM2 (Statistical Parametric Mapping 2, Institute of Neurology, London, http://www.fil.ion.ucl.ac.uk/spm/) running on Matlab (MathWorks Inc., Natick, MA, USA). Masking ROI maps (including the bilateral frontal lobes, parietal lobes, temporal lobes, occipital lobes, and limbic lobes; and the lenti-

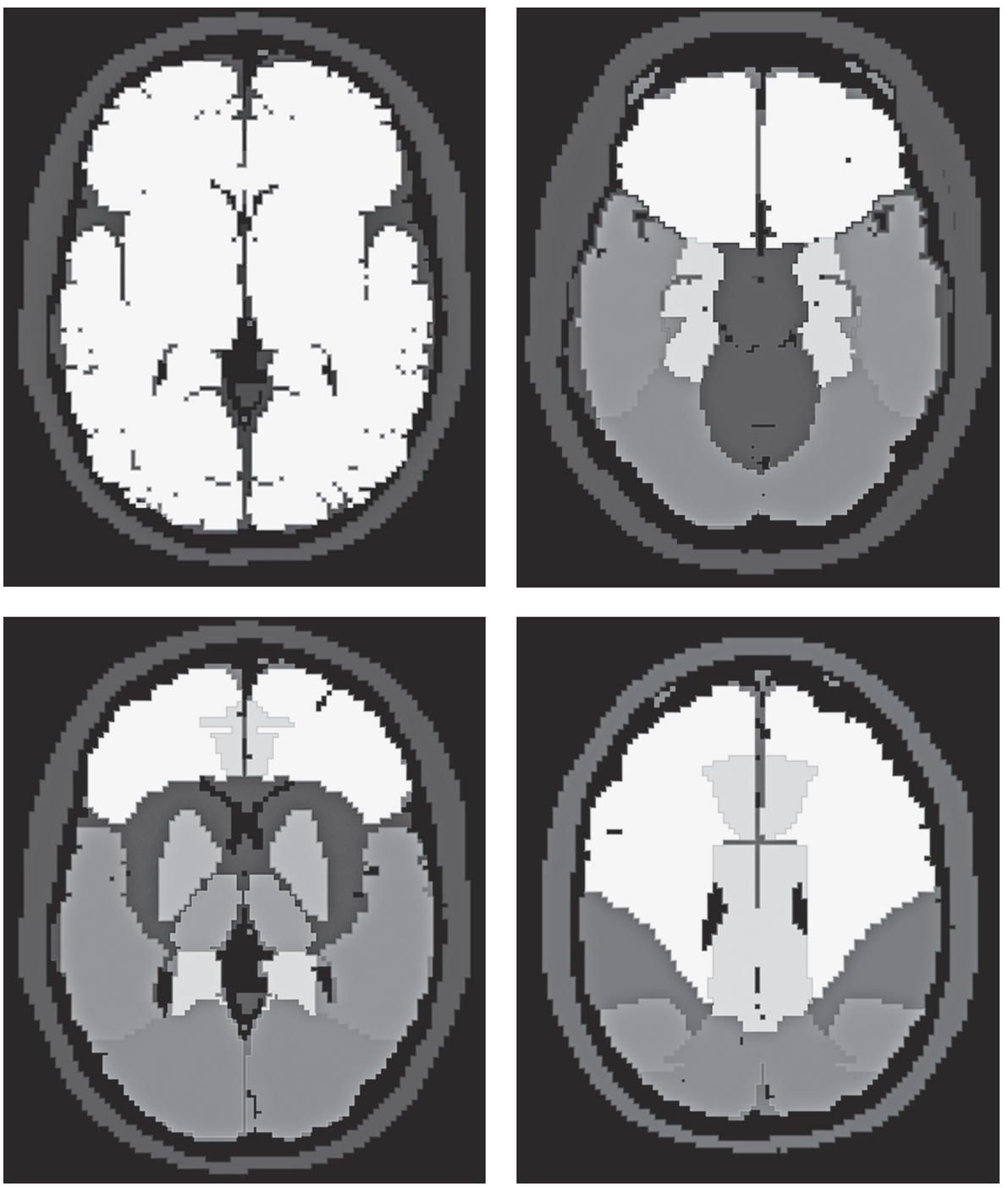

Figure 1 Normalized ROI maps of hemisphere (white areas on A) at the level of the basal ganglion, and the other regional areas at the level of the interpeduncular cistern (B), basal ganglion (C), and centrum semiovale (D) are shown. The areas on (B), (C), and (D) indicate frontal lobe, limbic lobe, lentiform nucleus, thalamus, temporal lobe, occipital lobe, and parietal lobe in the order of the gradient from white to black. Each ROI was separated and used for the calculation of the regional perfusion value.

form nucleus, thalamus, cerebellar hemisphere, and the brain stem) were created using the free add-on software WFU pickatlas (WFU PickAtlas, Joseph Maldjian, MD, Wake Forest University School of Medicine, North Carolina, USA, http://www.fmri.wfubmc.edu/download.htm)

Table 1 **Patient profiles**

Patient Number	**1**	**2**	**3**
age/sex	**60/F**	**73/F**	**64/M**
Chief complaint	Difficulty in conversation Aprophoria	Bilateral conjunctival hyperemia	General tonic convulsion Small hemorrhage on right temporal lobe
Shunt area	Torcular Hemophili -left transverse -sigmoid sinus	Bilateral cavernous sinuses	Right transverse -signmoid sinus
Classification	Cognard type II a+b Lalwani grade 3	Cognard type II a+b Barrow type D	Cognard type II a+b Lalwani grade 3
Feeding arteries	Bilateral occipital arteries Left posterior auricular artery Left middle meningeal artery Left accessory meningeal artery	Bilateral ascending pharyngeal arteries Bilateral middle meningeal arteries Bilateral meningohypophyseal arteries	Bilateral occipital arteries Right posterior auricular artery Right middle meningeal artery Left ascending pharyngeal artery
Draining course	Left superior petrosal -cavernous sinus -cortical vein (retrograde) Left Labbe's vein (retrograde) Right transverse -sigmoid sinus (antegrade)	bilateral superior ophthalmic veins (retrograde) left inferior ophthalmic veins (retrograde) Left uncal vein (retrograde) Basilar plexus (antegrade)	Right cerebellar hemispheric veins (retrograde) Temporo -parieto -occipital cortical veins (retrograde) Superior sagittal -left transverse -sigmoid sinus (antegrade) Straight-left transverse -sigmoid sinus (antegrade)
Treatment	Transcatheter arterial embolization	Transcatheter sinus coil embolization	Transcatheter arterial embolization and sinus coil embolization
Outcome	Improvement on MAIS-III test	Improvement in conjuctival hyperemia	No recurrence of convulsion
Period of ASL imaging acquisition	39th day before treatment 8POD* 112POD	11th day before treatment 20POD 120POD	19th day before treatment 19POD

**POD: postoperative day*

running on SPM2. The masking ROI maps were also normalized in the same processing as for normalization of ASL maps (Figure 1). The ASL values of all ROI were calculated with the normalized ASL maps and masking ROI maps by using ImageJ (Wayne Raqsband, National Institutes of Health, Bethesda, Maryland, USA, http://rsb.info.nih.gov/ij/index.html).

SPECT imaging

All SPECT studies were performed on days 4- 36 before treatment in all patients using a triple-head rotating gamma camera (Multi-SPECT 3, Siemens AG, Erlangen, Germany) with a fan-beam collimator. The spatial resolution was 5.7 mm full width at half maximum (FWHM) at 10 cm. The SPECT scans were initiated ten minutes after the intravenous injection of 600MBq of 99mTc-ethyl-cysteinate dimmer (ECD) (FUJIFILM RI Pharma Co., Ltd., Tokyo, Japan) in Patient 1, and 15 minutes after the intravenous injection of 167 MBq of 123I-N-isopropyl-p-iodoamphetamine (IMP) (Nihon Medi-Physics Co., Ltd., Nishinomiya, Japan) in Patients 2 and 3. The SPECT acquisition was undertaken in 30 steps (90 projections) with a circular camera orbit and a 1.23-fold zoom, and at each step, counts were collected for 40 seconds. Reconstruction of the images was performed by filtered back projection using Butterworth (order = 5, cutoff = 0.3 cycle/cm) and Ramp filters with Chang's attenuation

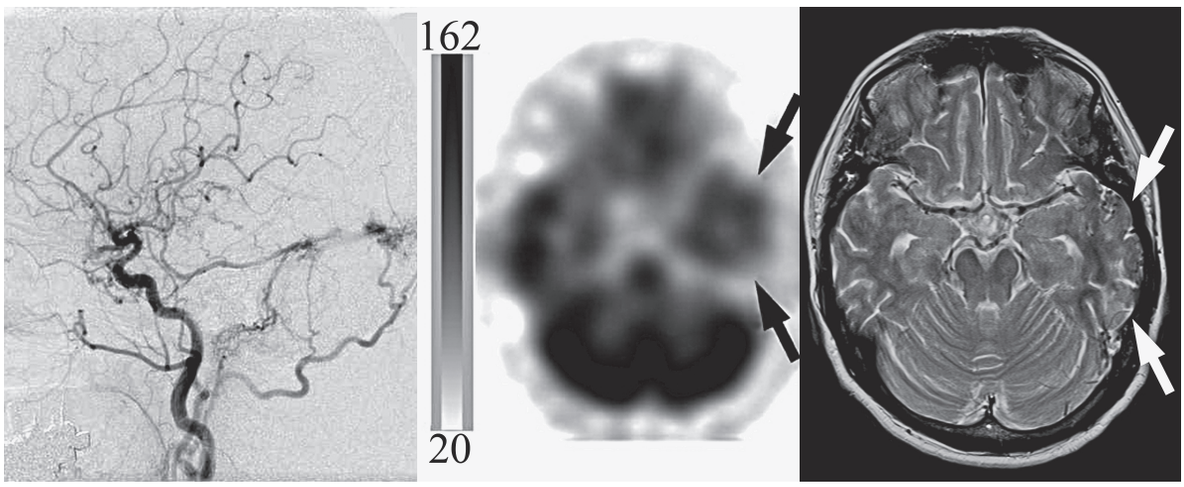

A B C

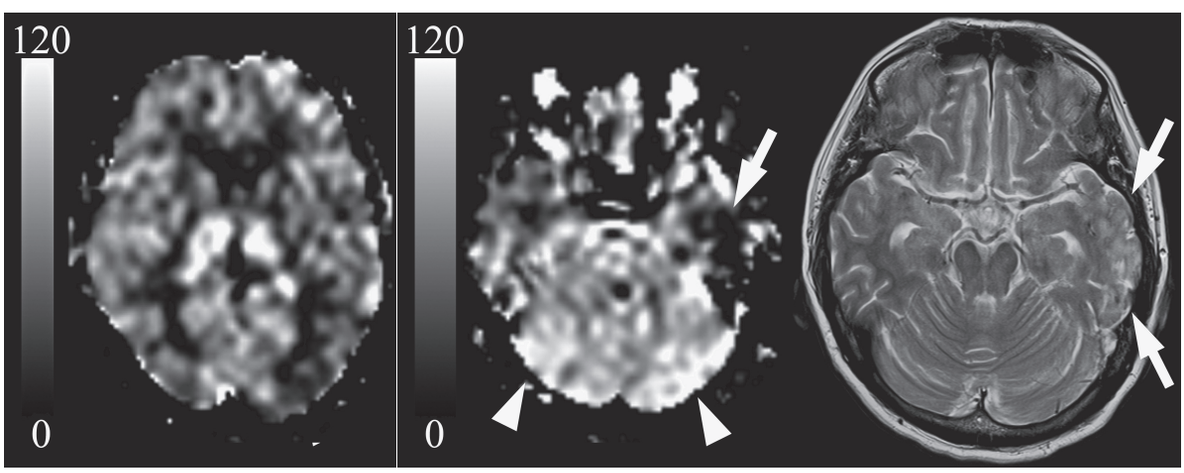

D E F

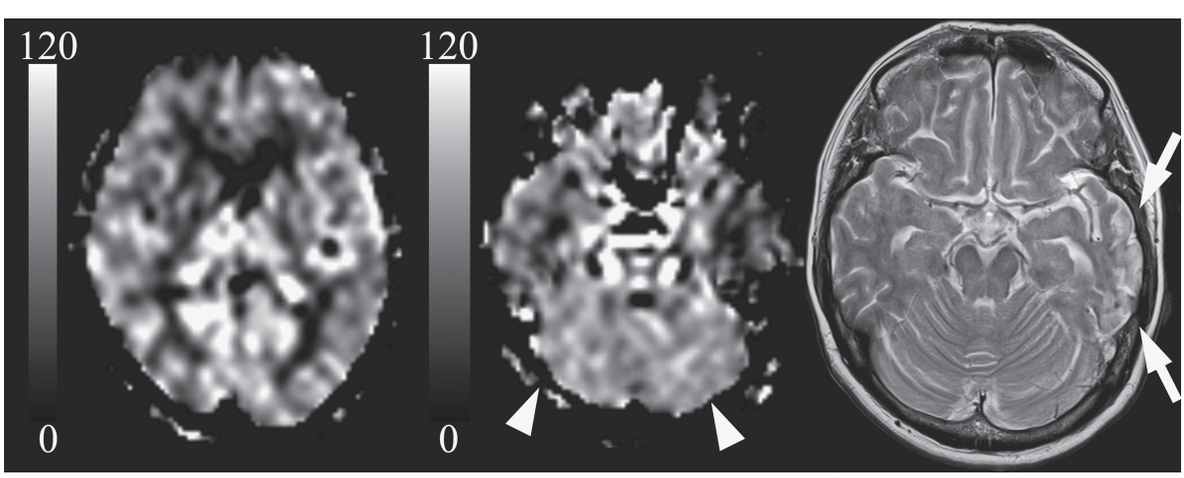

G H I

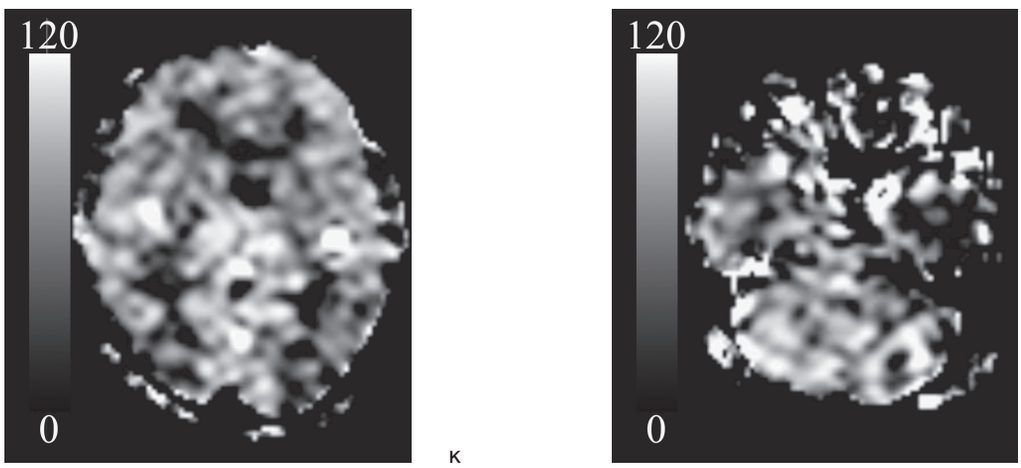

Figure 2 A 60-year-old woman with fistulas at the torcular Herophili-left transverse - sigmoid sinus (Cognard's IIa+b type/Lalwani's grade 3). Lateral view of the left external common carotid angiogram (A) showed the shunt flow from the occipital artery via fistulas at the torcular Herophili- left transverse - sigmoid sinus draining in a retrograde fashion into Labbe's vein. 99m-Tc ECD SPECT imaging with a gray scale (162 and 20 of the maximal and minimal gamma-ray counts, respectively) (B) demonstrated low perfusion in the left temporal lobe (arrow). T2-weighted image (C) demonstrated the high intensity with the flow void in the left temporal lobe, suggesting venous infarction with the retrograde venous reflux (arrow). ASL-MRI with a gray scale (120 and 0 of the maximal and minimal ASL values (mL / 100 g brain tissue / minute), respectively) before treatment (D, E) also showed hypointensity (arrow on E). However, there was a discrepancy in the bilateral cerebellar hemispheres, where hyperintensity was seen on ASL-MRI (arrowhead on E), but no abnormal findings were seen on SPECT imaging (arrowhead on B). On days 8-20 after treatment, T2-weighted image (F) revealed the disappearance of the flow void, suggesting the resolution of the retrograde venous reflux (arrow). The ASL values decreased in the bilateral cerebellar hemispheres (arrowhead on G), whereas ASL values increased in other regions (H) compared with those observed before treatment (D, E). On days 112-120 after treatment, T2-weighted image (I) showed the atrophic change and the sustainment of high intensity in the left temporal lobe (arrow). Lower ASL values were observed in all regions (J, K), as compared to those before treatment in the corresponding regions.

correction (0.02/cm). The matrix and pixel sizes of the SPECT images were 128×128 and 2.89×2.89×5.78 mm, respectively.

Digital subtraction angiography

Digital subtraction angiography (DSA) examinations were performed using a clinical angiography system (Axiom Artis TA; Siemens AG, Erlangen, Germany) on days 11-29 before treatment, day 0 for treatment, and days 10-16 after treatment. DSA of the bilateral common carotid arteries, internal carotid arteries, and external carotid arteries, and on either side of the vertebral artery was performed at least once for each patient during the pretreatment examination.

Data Analysis

Visual estimation of preoperative ASL images as compared to SPECT images

Preoperative ASL images were visually compared with SPECT images from each patient by two radiologists (a neuroradiologist (TN) with five years' experience and a nuclear medicine radiologist (TO) with five years experience) in consensus fashion. The ASL values for regions with abnormal findings were also considered to obtain more detailed information. Possible speculations for the findings were considered based on the DSA findings and ASL-MRI characteristics for the following reasons. Some previous reports have noted a relationship between abnormal cerebral perfusion and venous drainage pattern in cases of DAVFs [7,8]. On the other hand, the shunt blood flow through fistulas might affect ASL images since the arterial blood with less than 4 cm/s of flow velocity would be visualized.

Computerized analysis of temporal changes on serial ASL images

Increasing rates were calculated between pre- and post-treatment ASL values for all ROIs. Possible reasons for ASL value changes were attempted based on post-treatment DSA findings.

Results

Figure 2 shows the findings of patient 1 as a representative case.

Visual estimation of preoperative ASL-MRI compared with SPECT imaging

The following coincidences and discrepancies between ASL-MRI and SPECT imaging were identified. Additional speculations for these phenomenon were attempted in terms of the facts that ASL-MRI can reflect not only the parenchymal perfusion but also the arterial blood flow of 4 cm/s or less while SPECT imaging virtually corresponds to the parenchymal perfusion.

Regions of high perfusion on ASL-MRI but normal or low perfusion on SPECT imaging

High perfusion on ASL images was seen in regions where SPECT images showed either normal or low perfusion in the bilateral cerebellar hemisphere in patient 1, the pontomesencephalic marginal zone in patient 2, and the right cerebellar hemisphere in patient 3. Most of these regions in all three patients appeared to coincide with the fistula area on DSA. It seemed that ASL images reflected the shunt blood flow that accumulated directly in these regions while SPECT images reflected the normal or low perfusion in the brain tissue.

Regions of low perfusion on both ASL-MRI and SPECT imaging

Low perfusion on both ASL and SPECT images were observed in the left temporal lobe in patient 1, and in the left lentiform nucleus in patient 2. In both cases, these regions showed the high intensity on T2-weighted images and the retrograde shunt flow drainage into the cortical veins on DSA. However, these regions were at some distance from the shunting points. On DSA, the shunt flows reached these regions later than the regions around fistulas. It might be possible that both ASL and SPECT images predominantly reflected the low perfusion in the brain tissue.

Regions of normal perfusion on ASL-MRI but low perfusion on SPECT imaging.

SPECT images revealed the low perfusion in the bilateral frontal lobes in patient 2, and in the

Table 2 **Temporal changes in ASL-values (mL/100g/min) on region-of-interests**

Patient Nos. 1 2 3 ROI1/Acquisition period Pretreatment 8POD2 112POD Pretreatment 20POD 120POD Pretreatment 19POD									
Right	Frontal lobe	44.3	49.9 (5.6)3	18.8 (-25.5)	30.8	48.9 (18.1)	30.1 (-0.7)	5.4	22.8 (17.3)
	Parietal lobe	40.1	48.5 (8.5)	20.0 (-20.1)	34.9	38.6 (3.7)	19.3 (-15.6)	4.1	8.8 (4.7)
	Temporal lobe	48.4	58.5 (10.2)	37.0 (-11.4)	45.9	58.0 (12)	37.0 (-8.9)	12.5	23.8 (11.3)
	Occipital lobe	49.2	67.8 (18.6)	30.4 (-18.8)	30.7	44.1 (13.4)	22.0 (-8.7)	10.5	15.6 (5)
	Limbic lobe	54.5	63.0 (8.4)	37.9 (-16.7)	43.3	56.4 (13.2)	33.6 (-9.7)	16.7	36.8 (20.1)
	Lentiform nucleus	47.7	49.3 (1.6)	30.7 (-17)	54.2	44.6 (-9.6)	32.9 (-21.2)	21.1	50.3 (29.2)
	Thalamus	69.8	80.3 (10.4)	34.8 (-35)	69.4	50.2 (-19.2)	35.4 (-34)	27.8	49.5 (21.6)
	Cerebellum	72.7	70.2 (-2.5)	47.9 (-24.8)	56.0	44.3 (-11.7)	41.1 (-14.8)	42.7	42.7 (0)
	Brain stem	77.2	79.3 (2.1)	55.1 (-22.1)	82.9	60.6 (-22.4)	51.1 (-31.9)	15.0	52.5 (37.5)
Left	Frontal lobe	43.7	53.9 (10.2)	31.2 (-12.5)	23.3	47.0 (23.7)	30.7 (7.4)	14.3	28.3 (14)
	Parietal lobe	38.5	50.3 (11.7)	31.8 (-6.8)	37.1	41.8 (4.7)	21.0 (-16.1)	5.6	11.6 (6.1)
	Temporal lobe	40.4	51.1 (10.7)	36.9 (-3.6)	41.5	50.7 (9.2)	38.1 (-3.3)	13.1	31.0 (18)
	Occipital lobe	44.4	66.5 (22.1)	30.6 (-13.8)	29.4	39.5 (10.1)	23.2 (-6.2)	3.7	11.6 (7.9)
	Limbic lobe	48.3	59.0 (10.7)	42.6 (-5.7)	43.0	48.6 (5.6)	34.7 (-8.2)	15.5	38.4 (22.9)
	Lentiform nucleus	42.2	53.5 (11.3)	28.8 (-13.5)	30.6	50.7 (20.1)	24.7 (-5.9)	28.8	40.5 (11.7)
	Thalamus	62.4	69.5 (7.2)	30.3 (-32.1)	53.9	40.6 (-13.3)	33.3 (-20.6)	28.5	50.4 (21.9)
	Cerebellum	71.3	67.7 (-3.6)	46.7 (-24.6)	54.9	47.2 (-7.8)	33.1 (-21.9)	25.6	35.5 (9.8)
	Brain stem	75.4	78.6 (3.3)	42.8 (-32.6)	84.0	71.3 (-12.7)	61.3 (-22.7)	24.0	56.4 (32.4)

[1] ROI: region-of-interest, [2] POD: postoperative day, [3] ( ): the difference from the ASL-value pretreatment.

right temporo-parieto-occipital lobe in patient 3, whereas no abnormal findings were found on ASL images in either case. On the other hand, in patient 3, the right temporo-occipital lobe demonstrated a high intensity on T2WI and plenty of shunt blood flow on DSA. Thus, SPECT images might indicate the extensively lower perfusion (i.e., interruption of flow due to venous congestion) than that suggested by DSA. It should be noted that an equation between the abundant shunt flow versus the parenchymal low perfusion in those regions might yield a symmetrical appearance on ASL images.

Computerized analysis of temporal changes in serial ASL images

Table 2 shows temporal changes in ASL values in all ROI. The following observations and speculations for those were described.

8-20 days after treatment in all patients

At 8-20 days after treatment, ASL values in the regions around shunting points remained the same or decreased in all patients, i.e. in the bilateral cerebellar hemispheres in patient 1; in the right lentiform nucleus, bilateral thalami, bilateral cerebellar hemispheres, and the brain stem in patient 2; and the ASL values remained unchanged in the right cerebellar hemisphere in patient 3. On DSA, a reduction in shunt flow and an effacement of retrograde venous drainage were observed after treatment in all patients. Decreases in ASL values in these areas appeared to be associated with the corresponding decrease in shunt flow.

On the contrary, the ASL values in the regions other than the shunting points increased in all patients. These findings may reflect a transient excessive hyperperfusion caused by the resolution of the venous congestion and the post treatment hyperperfusion.

112 and 120 days after treatment in patients 1 and 2

On days 112 and 120 after treatment, patients 1 and 2 had lower ASL values in all regions compared to those in the same regions prior to treatment. These findings seemed to reflect the recovery of autoregulation and the stable supply of the blood flow, both of which would be expected to facilitate a return to the normal state of the brain perfusion. This speculation, however, could not be certified because no DSA examinations were performed around days 112 and 120 in either of those patients.

Discussion

Dural arteriovenous fistulas (DAVFs) are well-known to be associated with brain hemorrhage or venous infarction due to the impediments of the normal venous perfusion [2,4,24]. The abundant arterial blood flow via arteriovenous shunts, steno-occlusive changes in the sinuses, and the subsequent abnormal retrograde venous drainage were thought as the main pathological factors.

Some patients with DAVFs have been reported to develop the symptoms such as the progressive dementia, Parkinsonism, or other disorders of higher-brain function [5,6]. The pathologic areas for these symptoms showed the low perfusion on brain SPECT imaging and improved after proper treatment. Early diagnosis and treatment are important to avoid the development of secondary neurological deficits caused by DAVFs [5].

Two patients with DAVFs were previously reported to have developed pathological high perfusion after treatment [13,25]. One had a treatable headache, but the other experienced frequent generalized convulsions, which resulted in slight disorientation sequelae. A number of factors could potentially contribute to the development of the high perfusion, including vasoparalysis in regions with impaired autoregulation, a rapid resolution of the venous hypertension, and delays in the treatment.

Evaluations of intracranial hemodynamics will be quite important to elucidate the pathological context. However, the detailed etiological mechanisms have not been fully elucidated. A small number of institutions with nuclear medicine facilities and a high examination cost are just two of many practical limitations. While ASL-MRI as a quantitative perfusion MRI has some problems that remain to be resolved, it also has several advantages including the noninvasive procedure, the frequently repeatable examination, and the high cost-benefit. Thus, ASL-MRI may provide a useful adjunct tool for resolving diagnostic and methodological questions about cerebral perfusion images. Thus far, ASL-MRI has been demonstrated to be reliable and its results reproducible in the assessment of cerebral blood flow (CBF) in various pathological states, including cerebrovascular disease [26-28], neurodegenerative disease [29,30], and temporal lobe epilepsy [31,32]. However, to date there have been no clinical studies of DAVF using ASL imaging.

The most noteworthy finding of the present study was the visualization of shunt flow. This is because ASL-MRI could visualize blood flow in any places including arteries, veins, or parenchyma as far as it was less than 4 cm/s of flow velocity. The sensitivity of ASL images for shunt blood flow may confound the proper quantification of brain perfusion in DAVF cases. However, ASL images may be useful for detecting shunt flow, which in turn might facilitate monitoring responses to treatment and noninvasively following patients for recurrence.

ASL images of DAVFs before and after treatment were investigated, and the following findings suggested a number of diagnostic possibilities. Most regions around shunt-flow areas had high ASL values, whereas SPECT images revealed no abnormalities or low perfusion in all patients in those same areas. Generally, ASL images allow the tracing of intracranial flow. In the brain, high ASL values may predominantly reflect abundant arterial shunt flow via fistulas, rather than perfusion blood flow in regions of interest. In other regions not involving shunting, ASL values would be expected to vary based on one or more of the following: blood flow disturbances due to venous congestion, the volume and transit time of shunting inflow, and/or increases in the autoregulation of brain perfusion. Decreases in ASL values in these regions on days 8-20 after treatment appeared to correspond to decreases in shunt flow. However, the ASL values in the regions other than those involving shunting increased in all three patients. These findings may reflect a transient high perfusion caused by resolution of the venous congestion and maintenance of the increase in regulation of brain perfusion after treatment. On days 112 and 120 after treatment, patients 1 and 2 had lower ASL values in all ROI, as compared to those before treatment, which seemed to reflect a recovery of autoregulation and a stable supply of blood flow, both of which would be expected to facilitate a return to a normal state of perfusion. Although there were no specific findings on DSA, ASL values might be more revealing, i.e., they might remain the same or decrease compared with values observed before treatment. There are some clear limitations of the present study, in particular the small sample size and the short duration of surveillance. In addition, the three patients examined here were all in a critical condition, and all presented with cerebral perfusion abnormalities on SPECT images. Patients with less severe disease should be examined in future studies of DAVFs. Moreover, no method is currently available for the objective evaluation of individual ASL images. Statistical analyses of data from a database of normal ASL images would be desirable. Whereas the serial ASL images studies of the three patients described here were highly suggestive, the findings do not provide sufficient support for our hypothesis that ASL images reflect a combination of shunt flow, venous congestion, and the autoregulation of brain perfusion. In particular, it may not necessarily be denied that ASL-MRI acquisition and post-processing method including the quantification fail since they have not been fully validated yet. Further studies will therefore be needed to confirm this and other hypotheses.

Conclusions

The pre-treatment ASL images studies of all three patients with DAVFs demonstrated hyperintensity in regions surrounding shunting areas, in which no abnormalities were detected on SPECT images. It is possible that ASL images could be useful for revealing abundant arterial shunt flow via fistulas.

The ASL values in the regions surrounding shunting areas in all three patients remained the same or decreased, while the ASL values of other regions increased on days 8-20 after treatment. This was thought to be due to a decrease in shunt flow volume, an improvement in venous congestion, and a maintained increase in the autoregulation of brain perfusion. All regional ASL values decreased on days 112 and 120 in two patients, which might have been a reflection of decreased autoregulation. Thus, ASL images could potentially enhance our understanding of the detailed hemodynamic changes associated with DAVFs before and after treatment.

Acknowledgement

This work was supported by a Grant-in-Aid from the Japanese Society of Neuroradiology.

References

1 Newton TH, Cronqvist S. Involvement of dural arteries in intracranial arteriovenous malformations. Radiology. 1969; 93: 1071-1078.
2 Awad IA, Little JR, Akarawi WP, et al. Intracranial dural arteriovenous malformations: factors predisposing to an aggressive neurological course. J Neurosurg. 1990; 72: 839-850.
3 Duffau H, Lopes M, Janosevic V, et al. Early rebleeding from intracranial dural arteriovenous fistulas: report of 20 cases and review of the literature. J Neurosurg. 1999; 90: 78-84.
4 Hurst RW, Bagley LJ, Galetta S. Dementia resulting from dural arteriovenous fistulas: the pathologic findings of venous hypertensive encephalopathy. Am J Neuroradiol. 1998; 19: 1267-1273.
5 Waragai M, Takeuchi H, T. Fukushima T, et al. MRI and SPECT studies of dural arteriovenous fistulas presenting as pure progressive dementia with leukoencephalopathy: a cause of treatable dementia. Eur J Neurol. 2006; 13: 754-759.
6 Matsuda S, Waragai M, Shinotoh H, et al. Intracranial dural arteriovenous fistula (DAVF) presenting as progressive dementia and Parkinsonism. J Neurol Sci. 1999; 165: 43-47.
7 Kai Y, Hamada J, Morioka M, et al. Pre- and post-treatment MRI and single photon emission CT in patients with dural arteriovenous fistulas and retrograde leptomeningeal venous drainage. Am J Neuroradiol. 2003; 24: 619-625.
8 Kai Y, Hamada J, Morioka M. Correlation between magnetic resonance images and draining patterns in dural arteriovenous fistulas with leptomeningeal venous drainage. Acta Neurochir. 2000; 142: 413-418.
9 Awad IA, Little JR, Akarawi WP. Intracranial dural arteriovenous malformations: factors predisposing to an aggressive neurological course. J Neurosurg. 1990; 72: 839-850.
10 Lasjaunias P, Chiu M, ter Brugge K. Neurological manifestations of intracranial dural arteriovenous malformations. J Neurosurg. 1986; 64: 724-730.
11 Iwama T, Hashimoto N, Takagi Y. Hemodynamic and metabolic disturbances in patients with intracranial dural arteriovenous fistulas: positron emission tomography evaluation before and after treatment. J Neurosurg. 1997; 86: 806-811.
12 Kawaguchi T, Fujita S, Yamada H. Hemodynamics before and after the total removal of a dural arteriovenous malformation of the posterior fossa: case report. Surg Neurol. 1988; 30: 457-461.
13 Kuroda S, Ushikoshi S, Houkin K. Postoperative hyperperfusion in dural arteriovenous fistula associated with venous ischemia: case report. Surg Neurol. 1998; 49: 406-411.
14 Willinsky R, Terbrugge K, Montanera W. Venous congestion: an MR finding in dural arteriovenous malformations with cortical venous drainage. Am J Neuroradiol. 1994; 15: 1501-1507.
15 Detre JA, Leigh JS, Williams DS, Koretsky AP. Perfusion imaging. Magn Reson Med. 1992; 23 (1): 37-45.
16 Wong EC, Buxton RB, Frank LR. Quantitative imaging of perfusion using a single subtraction (QUIPSS and QUIPSS II). Magn Reson Med. 1998; 39 (5): 702-708.
17 Kim SG. Quantification of relative cerebral blood flow change by flow-sensitive alternating inversion recovery (FAIR) technique: application to functional mapping. Magn Reson Med. 1995; 34 (3): 293-301.
18 Petersen ET, Lim T, Golay X. Model-free arterial spin labeling quantification approach for perfusion MRI. Magn Reson Med. 2006; 55 (2): 219-232.
19 Luh WM, Wong EC, Bandettini PA, et al. QUIPSS II with thin-slice TI1 periodic saturation: a method for improving accuracy of quantitative perfusion imaging using pulsed arterial spin labeling. Magn Reson Med. 1999; 41: 1246-1254.
20 Noguchi T, Yoshiura T, Hiwatashi A, et al. Quantitative perfusion imaging with pulsed arterial spin labeling: a phantom study. Magn Reson Med Sci. 2007; 6: 91-97.
21 Noguchi T, Yoshiura T, Hiwatashi A, et al. Perfusion imaging of brain tumors using arterial spin labeling: correlation with histopathologic vascular density. Am J Neuroradiol. 2008; 29(4): 688-693.
22 Petersen ET, Lim T, Golay X. Model-free arterial spin-labeling quantification approach for perfusion MRI. Magn Reson Med. 2006; 55(2): 219-232.
23 Wang J, Licht DJ, Jahng GH, et al. Pediatric perfusion imaging using pulsed arterial spin-labeling. J Magn Reson Imaging. 2003; 18(4): 404-413.
24 Kai Y, Hamada J, Morioka M, et al. Postoperative hyperperfusion in a patient with a dural arteriovenous fistula with retrograde leptomeningeal venous drainage: case report. Neurosurgery. 2003; 53 (1): 228-232.
25 Chalela JA, Alsop DC, Gonzalez-Atavales JB, et al. Magnetic resonance perfusion imaging in acute ischemic stroke using continuous arterial spin-labeling. Stroke. 2000; 31: 680-687.
26 Kimura H, Kado H, Koshimoto Y, et al. Multislice continuous arterial spin-labeled perfusion MRI in patients with chronic occlusive cerebrovascular disease: a correlative study with CO2 PET validation. J Magn Reson Imaging. 2005; 22: 189-198.
27 Detre JA, Alsop DC, Vives LR, et al. Noninvasive MRI evaluation of cerebral blood flow in cerebrovascular disease. Neurology. 1998; 50: 633-641.
28 Alsop DC, Detre JA, Grossman M. Assessment of cerebral blood flow in Alzheimer's disease by spin-labeled magnetic resonance imaging. Ann Neurol. 2000; 47: 93-100.
29 Du AT, Jahng GH, Hayasaka S, et al. Hypoperfusion in frontotemporal dementia and Alzheimer disease by arterial spin-labeling MRI. Neurology. 2006; 67: 1215-1220.
30 Liu HL, Kochunov P, Hou J, et al. Perfusion-weighted imaging of interictal hypoperfusion in temporal lobe epilepsy using FAIR-HASTE: comparison with H215O PET measurements. Magn Reson Med. 2001; 45: 431-435.
31 Wolf RL, Alsop DC, Levy-Reis I, et al. Detection of mesial temporal lobe hypoperfusion in patients with temporal lobe epilepsy by use of arterial spin labeled perfusion MR imaging. Am J Neuroradiol. 2001; 22: 1334-1341.

Tomoyuki Noguchi, MD
Department of Radiology, and *Neurosurgery
Faculty of Medicine
Saga University
5-1-1, Nabeshima, Saga
849-8501, Japan
Tel.: 81-952-34-2309
Fax: 81-952-34-2016
E–mail: tnogucci@radiol.med.kyushu–u.ac.jp